

DISTANCE TO THE LOW-VELOCITY CLOUD IN THE DIRECTION OF THE HIGH-VELOCITY COMPACT
CLOUD CO-0.40-0.22

YUHEI IWATA,¹ HARUKA KATO,² DAISUKE SAKAI,^{3,4} AND TOMOHARU OKA^{1,2}

¹*School of Fundamental Science and Technology, Graduate School of Science and Technology, Keio University, 3-14-1 Hiyoshi, Kohoku-ku, Yokohama, Kanagawa 223-8522, Japan*

²*Department of Physics, Faculty of Science and Technology, Keio University, 3-14-1 Hiyoshi, Kohoku-ku, Yokohama, Kanagawa 223-8522, Japan*

³*Department of Astronomy, Graduate School of Science, The University of Tokyo, 7-3-1 Hongo, Bunkyo-ku, Tokyo 113-0033, Japan*

⁴*Mizusawa VLBI Observatory, National Astronomical Observatory of Japan, 2-12 Hoshi-ga-oka, Mizusawa-ku, Oshu-shi, Iwate 023-0861, Japan*

(Received March 7, 2017; Revised March 17, 2017; Accepted March 17, 2017)

Submitted to ApJ

ABSTRACT

CO-0.40-0.22 is a peculiar molecular cloud that is compact and has an extraordinary broad velocity width. It is found in the central molecular zone of our Galaxy. In this direction, there is another cloud with an H₂O maser spot at a lower velocity. Collision with this low-velocity cloud could be responsible for the broad velocity width of CO-0.40-0.22. We performed phase-referencing VLBI astrometry with VERA and detected the annual parallax of the H₂O maser spot in the low-velocity cloud to be 0.33 ± 0.14 mas, which corresponds to a distance of $3.07^{+2.22}_{-0.91}$ kpc from the Sun. This implies that the low-velocity cloud is located in the Galactic disk on the near side of the central molecular zone.

Keywords: astrometry — Galaxy: center — ISM: clouds — masers

arXiv:1703.08295v1 [astro-ph.GA] 24 Mar 2017

1. INTRODUCTION

Large-scale CO surveys of the central molecular zone (CMZ) of our Galaxy have detected a peculiar population of molecular clouds, namely, high-velocity compact clouds (HVCCs; Oka et al. 1998, 2007, 2012). HVCCs are characterized by their compact appearance ($d < 10$ pc) and unusually large velocity width ($\Delta V > 50$ km s⁻¹). Some of energetic HVCCs contain small expanding arcs and shells, indicating that local explosive events, such as supernova explosions, may be responsible for the origin of HVCCs (Oka et al. 1999, 2001, 2008; Tanaka et al. 2007).

However, a majority of HVCCs do not have any expanding features or counterparts at other wavelengths. CO-0.40-0.22 is such a featureless, energetic HVCC centered at $(l, b, V_{\text{LSR}}) = (-0^{\circ}40, -0^{\circ}22, -80$ km s⁻¹). It has a small size (~ 3 pc; Figure 1a) and an extremely broad velocity width (~ 100 km s⁻¹; Figure 1b). Intensive studies based on single-dish observations of molecular lines revealed that CO-0.40-0.22 consists of an intense component with a shallow velocity gradient and a less intense high-velocity wing. This behavior is interpreted as a gravitational kick to the molecular cloud caused by an invisible compact object with a mass of $\sim 10^5 M_{\odot}$ (Oka et al. 2016). This massive object could be an intermediate-mass black hole (IMBH), which would contribute to the evolution of the central supermassive black hole (SMBH; Ebisuzaki et al. 2001).

In the direction of CO-0.40-0.22, there is another molecular cloud at $V_{\text{LSR}} \sim +20$ km s⁻¹ (Figure 1b). This low-velocity cloud (LV cloud) is associated with a bright nebula of infrared emission, 22 GHz H₂O maser emission, and 6.7 GHz CH₃OH maser emission (Caswell et al. 1983; Chambers et al. 2014), indicating that massive star formation is taking place. Its physical relation to CO-0.40-0.22 is unclear. If the LV cloud is physically associated with CO-0.40-0.22, collision between these clouds with significantly different velocities induces intense shock, resulting in a broad velocity width feature, which bridges colliding clouds in the position-velocity space (e.g., Matsumura et al. 2012). To examine the cloud-cloud collision scenario for CO-0.40-0.22, the distance to the LV cloud should be determined directly.

2. OBSERVATIONS AND ANALYSIS

Observations of H₂O 6₁₆-5₂₃ (22.235080 GHz) maser in H₂O 359.62-0.25 were carried out in 12 epochs from

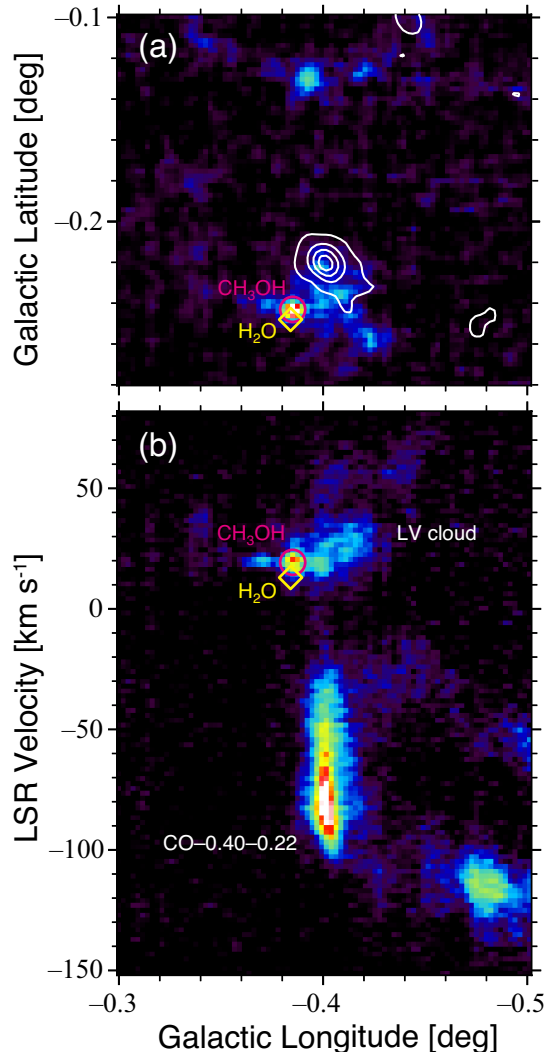


Figure 1. (a) Map of velocity-integrated HCN $J=4-3$ emission. The velocity ranges are taken from $V_{\text{LSR}} = 0$ to $+40$ km s⁻¹ (color) and $V_{\text{LSR}} = -120$ to 0 km s⁻¹ (contour). The intensity increases as the color changes from violet to white. The contour levels are 100, 300, 500, and 700 K km s⁻¹. The yellow diamond denotes the position of the 22 GHz H₂O maser spot at H₂O 359.62-0.25 (Caswell et al. 1983), while the magenta circle denotes that of the 6.7 GHz CH₃OH maser spot (Chambers et al. 2014). (b) Longitude-velocity map of HCN $J=4-3$ emission integrated over latitudes from $-0^{\circ}28$ to $-0^{\circ}20$. Yellow diamond and magenta circle denote the longitude and velocity of H₂O and CH₃OH maser spots, respectively.

November 2015 to January 2017 with VERA¹. Observational details are summarized in Table 1. The interval

¹ VLBI Exploration of Radio Astrometry (VERA) is a Japanese VLBI array for phase-referencing astrometry, consisting of four domestic stations equipped with dual-beamed radio telescopes.

Table 1. VERA Observations.

Epoch	Code	Date	Antennas Available ^a
1	r15332a	2015 Nov 28	MZ, IR, OG, IS
2	r15360a	2015 Dec 26	MZ, IR, OG, IS
3	r16026b	2016 Jan 26	MZ, IR, OG, IS
4	r16061e	2016 Mar 1	IR, OG, IS
5	r16084c	2016 Mar 24	IR, OG, IS
6	r16114b	2016 Apr 23	MZ, IR, OG, IS
7	r16142b	2016 May 21	MZ, IR, OG, IS
8	r16166a	2016 Jun 14	MZ, IR, OG, IS
9	r16236a	2016 Aug 23	MZ, IR, OG, IS
10	r16262a	2016 Sep 18	MZ, IR, OG, IS
11	r16327a	2016 Nov 22	MZ, IR, OG, IS
12	r17017a	2017 Jan 17	MZ, IR, OG, IS

^aAntenna codes are MZ: at Mizusawa, Iwate, IR: at Iriki, Kagoshima, OG: at Ogasawara Islands, Tokyo, and IS: at Ishigakijima, Okinawa.

of the observations was ~ 1 month. All four stations of VERA were utilized except for epochs 4 and 5. H₂O 359.62–0.25 and position reference source J1745–2820 ($\alpha_{J2000.0} = 17^{\text{h}}45^{\text{m}}52^{\text{s}}.4968$, $\delta_{J2000.0} = -28^{\circ}20'26''.294$) were observed simultaneously in the dual-beam mode. The tracking center position of H₂O 359.62–0.25 was set to ($17^{\text{h}}45^{\text{m}}39^{\text{s}}.0908$, $-28^{\circ}23'30''.218$). The separation angle between them was $1^{\circ}05'$. NRAO530 was also observed as a bandpass and delay calibrator every 40 min. The observation sequence in each day spanned ~ 3 h.

Left-handed circular polarization was received, sampled with 2-bit quantization. The signals were filtered using the VERA digital filter unit (Iguchi et al. 2005) to obtain 16 IF channels each with a bandwidth of 16 MHz. One IF channel was assigned to H₂O 359.62–0.25 and 15 IF channels to J1745–2820. The data were recorded onto magnetic tapes at a rate of 1024 Mbps. The system temperatures including atmospheric loss were measured to be 100–1000 K, depending on the stations and weather conditions. Correlation processing was conducted on the Mizusawa software correlator at the National Astronomical Observatory of Japan (NAOJ). The correlator accumulation period was 1 s. For the J1745–2820 data, the spectral resolution was 64 points per each 16 MHz channel. For the H₂O 359.62–0.25 data, the frequency resolution was 15.625 kHz, which corresponds to a velocity resolution of 0.21 km s^{-1} .

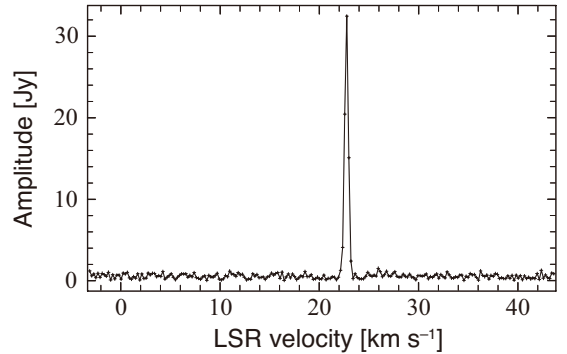


Figure 2. The cross-power spectrum of H₂O 359.62–0.25. This was obtained from the data on the sixth epoch at Mizusawa-Iriki baseline.

Data reductions were performed by using the NRAO Astronomical Image Processing System (AIPS). The amplitude was calibrated by the system noise temperatures, and bandpass calibration was made with the NRAO530 data. The dual-beam phase-calibration data and the modified delay-tracking model were applied for accurate measurements. For phase-referencing, we calibrated the clock parameters using NRAO530 and performed a fringe fitting on the maser spot in H₂O 359.62–0.25 because of the low intensity of J1745–2820 (~ 70 mJy). The solutions were applied to the J1745–2820 data. We obtained the image of J1745–2820 by using task IMAGR. The position of J1745–2820 with respect to the H₂O maser spot was determined by elliptical Gaussian fitting to the brightness peak of the image. Since the position of J1745–2820 should be stable, we can regard the positional change of J1745–2820 as that of the H₂O maser spot.

3. RESULTS

H₂O 6₁₆–5₂₃ maser line was detected from H₂O 359.62–0.25 at $V_{\text{LSR}} \sim +22.7 \text{ km s}^{-1}$ in the first eight epochs (Figure 2). Only one spot (named ‘A’) was visible during epochs 1–5, while another spot (named ‘B’) appears at ~ 20 mas northeast of spot A during epochs 6–8 (Figure 3). We traced the position of spot A with respect to J1745–2820. Since spot B was more intense than A during epochs 6–8, we traced it with respect to J1745–2820. This was because we used the H₂O 359.62–0.25 data for the fringe fitting process. For this reason, we added the positional offset between spots A and B to obtain the accurate position of spot A.

Figure 4 shows the results of the position measurements of maser spot A. The position offsets are with respect to the average position of epochs 1–8. As shown in Figure 4, we detected the movement of spot A, particularly in the R.A. plot, which certainly deviates from a linear motion. The deviation seems to be a sinusoidal,

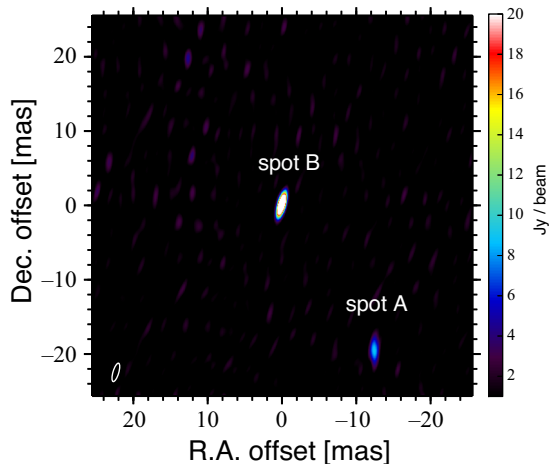


Figure 3. Phase-referenced image of the H₂O maser spots of $V_{\text{LSR}} = 22.7 \text{ km s}^{-1}$ at the sixth epoch. Maser spot A was visible during epochs 1–8, while spot B was visible during epochs 6–8. The coordinate offsets are with respect to the position of spot B ($\alpha_{\text{J2000.0}} = 17^{\text{h}}45^{\text{m}}39^{\text{s}}.0918$, $\delta_{\text{J2000.0}} = -29^{\circ}23'30''.207$). The synthesized beam is shown in the bottom left corner.

annual modulation. This must be due to the annual parallax of the maser spot. We derived the annual parallax and proper motions using both the R.A. and Dec. data simultaneously. Table 2 summarizes the best-fitting result. The obtained annual parallax and proper motions are $0.33 \pm 0.14 \text{ mas}$ and $1.31 \pm 0.33 \text{ mas yr}^{-1}$ for R.A. and $-2.41 \pm 0.87 \text{ mas yr}^{-1}$ for Dec., respectively. We employed a uniform weighting in the fitting procedure, because systematic errors are considerably larger than the statistical errors in the VLBI observations. We evaluated the systematic errors to be 0.16 mas in R.A. and 0.43 mas in Dec. A worse astrometric accuracy in Dec. can be seen in low-elevation angle sources, such as Galactic center sources, caused by an atmospheric zenith delay residual (Honma et al. 2008). The derived parallax corresponds to a distance of $3.07_{-0.91}^{+2.22} \text{ kpc}$ from the Sun.

4. DISCUSSION AND SUMMARY

The derived distance from the Sun corresponds to a Galactocentric distance of $5.26_{-2.22}^{+0.91} \text{ kpc}$ if we assume $R_0 = 8.33 \text{ kpc}$ (Gillessen et al. 2009). This shows that H₂O 359.62–0.25, as well as the LV cloud, is not in the CMZ. Assuming the normal distribution of the observed parallax, we obtained the probability that H₂O 359.62–0.25 is located further than 8 kpc to be 6.3%. Thus, the LV cloud is not in the CMZ with a confidence level of greater than 93.7%.

Figure 5 shows the line-of-sight location of the LV cloud. The most likelihood value $R_{\text{G}} = 5.92 \text{ kpc}$ falls on the Scutum-Crux arm. On the other hand, the velocity of the LV cloud ($V_{\text{LSR}} \sim +20 \text{ km s}^{-1}$) implies that the

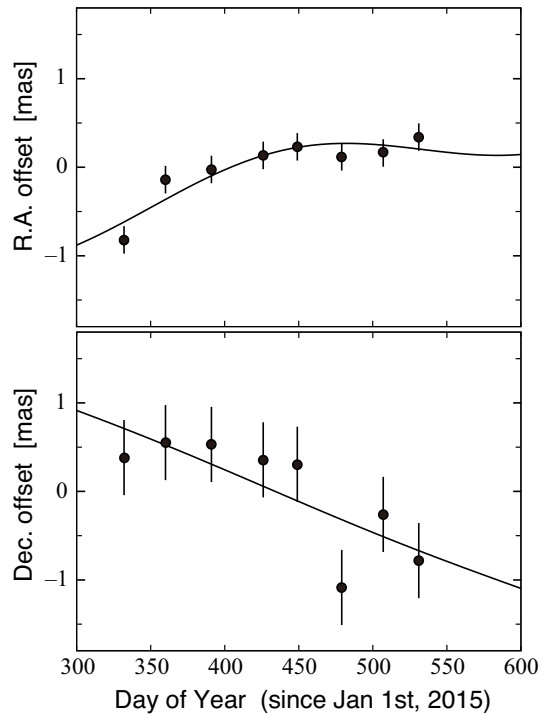


Figure 4. Positional variations of H₂O maser spot A. The top figure is for the R.A. direction and the bottom figure is for the Dec. direction. The solid lines are the best-fitting models including the annual parallax and the linear proper motion. Errors are the standard deviations from the best-fit curves. The position offsets are with respect to the average position of epochs 1–8 ($\alpha_{\text{J2000.0}} = 17^{\text{h}}45^{\text{m}}39^{\text{s}}.0908$, $\delta_{\text{J2000.0}} = -29^{\circ}23'30''.226$).

LV cloud may belong to the 4 kpc molecular ring (Sofue 2006), which is also within the 1σ uncertainty range. The LV cloud could be a member of the OB association responsible for RCW 137, which is a large (diameter $\sim 0^{\circ}.3$) HII region centered at $(l, b) = (-0^{\circ}.2, -0^{\circ}.2)$ (Rodgers et al. 1960). RCW 137 is visible in the optical wavelength, indicating a distance of $\lesssim 3 \text{ kpc}$ from the Sun. All these facts support the near distance of the LV cloud.

Our parallax measurement of H₂O 359.62–0.25 concludes that the LV cloud is in the Galactic disk on the near side of the CMZ. On the other hand, CO–0.40–0.22 is supposed to be in the CMZ by its extraordinary broad velocity width. An absorption feature in CO lines at $V_{\text{LSR}} \sim -50 \text{ km s}^{-1}$ (Oka et al. 2012) indicates that CO–0.40–0.22 is certainly behind the 3 kpc expanding arm (Sofue 2006). Therefore, the LV cloud is irrelevant to CO–0.40–0.22. The cloud-cloud collision scenario seems to be not applicable to the CO–0.40–0.22 case. We supposed another formation scenario for CO–0.40–0.22, a gravitational kick by a massive, point-like

Table 2. The best-fitting values of Parallax π and proper motions $\mu_\alpha \cos \delta$ and μ_δ .

V_{LSR} (km s $^{-1}$)	π (mas)	Distance (kpc)	$\mu_\alpha \cos \delta$ (mas yr $^{-1}$)	μ_δ (mas yr $^{-1}$)
+22.7	0.33 ± 0.14	$3.07^{+2.22}_{-0.91}$	1.31 ± 0.33	-2.41 ± 0.87

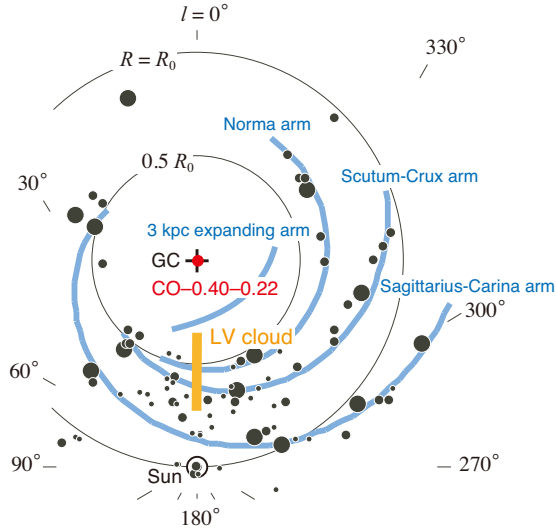


Figure 5. Locations of CO-0.40-0.22 and the LV cloud on the Galactic plane. Orange solid line indicates the derived distance of the LV cloud with 1σ uncertainty. Blue solid lines indicate the spiral arms of our Galaxy. The shapes of the spiral arms except for the 3 kpc expanding arm were obtained by fitting logarithmic spirals to high-excitation parameter HII regions. Black filled circles indicate the loci of the HII regions, with their sizes representing the excitation classification as described in Georgelin & Georgelin (1976). The shape of the 3 kpc expanding arm was obtained from an artist’s conception of the Milky Way (R. Hurt: NASA/JPL-Caltech/SSC).

object, which could be an IMBH (Oka et al. 2016). In summary, this annual parallax study ruled out at least one formation scenario other than the gravitational kick scenario.

We are grateful to all VERA staff members for operation of the telescope and the data correlation. The data analysis was in part carried out on the open use data analysis computer system at the Astronomy Data Center (ADC) of the NAOJ. We thank the anonymous referee for helpful comments. T.O. acknowledges support from JSPS Grant-in-Aid for Scientific Research (B) No. 15H03643.

REFERENCES

- Caswell, J. L., Batchelor, R. A., Forster, J. R., & Wellington, K. J. 1983, *Australian Journal of Physics*, 36, 401
- Chambers, E. T., Yusef-Zadeh, F., & Ott, J. 2014, *A&A*, 563, A68
- Ebisuzaki, T., Makino, J., Tsuru, T. G., et al. 2001, *ApJL*, 562, L19
- Georgelin, Y. M., & Georgelin, Y. P. 1976, *A&A*, 49, 57
- Gillessen, S., Eisenhauer, F., Trippe, S., et al. 2009, *ApJ*, 692, 1075
- Honma, M., Tamura, Y., & Reid, M. J. 2008, *PASJ*, 60, 951
- Iguchi, S., Kurayama, T., Kawaguchi, N., & Kawakami, K. 2005, *PASJ*, 57, 259
- Matsumura, S., Oka, T., Tanaka, K., et al. 2012, *ApJ*, 756, 87
- Oka, T., Hasegawa, T., Sato, F., Tsuboi, M., & Miyazaki, A. 1998, *ApJS*, 118, 455
- Oka, T., Hasegawa, T., Sato, F., Tsuboi, M., & Miyazaki, A. 2001, *PASJ*, 53, 787
- Oka, T., Hasegawa, T., White, G. J., et al. 2008, *PASJ*, 60, 429
- Oka, T., Mizuno, R., Miura, K., & Takekawa, S. 2016, *ApJL*, 816, L7
- Oka, T., Nagai, M., Kamegai, K., Tanaka, K., & Kuboi, N. 2007, *PASJ*, 59, 15
- Oka, T., Onodera, Y., Nagai, M., et al. 2012, *ApJS*, 201, 14

- Oka, T., White, G. J., Hasegawa, T., et al. 1999, ApJ, 515,
249
- Rodgers, A. W., Campbell, C. T., & Whiteoak, J. B. 1960,
MNRAS, 121, 103
- Sofue, Y. 2006, PASJ, 58, 335
- Tanaka, K., Kamegai, K., Nagai, M., & Oka, T. 2007,
PASJ, 59, 323